Supporting Information

Fu et al. 10.1073/pnas.1408836111

SI Materials and Methods

Cloning, Expression, and Purification. Full-length human RRS (residues 1–660) and AIMP1 (residues 1–312) genes were inserted simultaneously into pETDuet vector. Full-length human QRS (residues 1–775) was inserted into the pET28a vector. Both QRS and RRS contained a His6 tag at the N terminus. The plasmids containing the RRS gene, the AIMP1 gene, and the QRS gene were cotransformed into *E. coli* Rosetta (DE3), and the bacteria were grown in LB broth medium. Initially, the protein complexes were purified by an Ni^{2+} column using an imidazole gradient in 25 mM Tris·HCl (pH7.5), 300 mM NaCl, 5 mM 2-mercaptoethanol, and 5% glycerol. The eluted protein complex was purified further with an ion-exchange column (Mono-Q) followed by gel filtration on a Superdex 200 column equilibrated with 25 mM Tris·HCl (pH7.5), 150 mM NaCl, 5 mM DTT, and 5% glycerol. The RQA1 complex used for crystallization was concentrated to 15 mg/mL. To analyze the subcomplex formation by gel-filtration chromatography, full-length human KRS (residues 1–597) and AIMP2 (residues 1–320) were cloned into pET28a. Full-length human AIMP1 (residues 1–312) and RRS (residues 1–660) also were inserted into pCDF and pET21a, respectively, for biochemical analyses.

Crystallization and Data Collection. Crystals of the RQA1 complex were grown at 18 °C using the hanging-drop vapor-diffusion method from 5–10% methyl-pentene-diol, 0.1 M Tris·HCl (pH 7.4), 0.2 M NaCl. Diffraction data were collected at −170 °C using crystals flash-frozen in crystallization buffer containing 30% (wt/vol) glycerol. The crystals belong to space group $C222_1$ with dimensions of a = 102.7 Å, b = 313.3 Å, and c = 161.8 Å and contained one complex in the asymmetric unit. Diffraction data from native crystals were collected at 0.9795 Å on beamline 5C at the Pohang Advanced Light Source (Pohang, South Korea) and Photon Factory (Japan). The datasets were processed using the HKL2000 program (1).

Gel-Filtration Analyses. To determine whether AIMP1 or RRSs form the ternary complex, size-exclusion chromatography experiments for AIMP1 (M1–M4) and RRS (R1 or R2) mutants were performed in the presence of wild-type counterparts using a Superdex 200 16/60 column (GE Healthcare) at 4 °C. Running buffer contained 25 mM Tris·HCl (pH 7.5), 150 mM NaCl, 5 mM DTT, and 5% glycerol. The three (RRS, QRS, and AIMP1) or five (RRS, QRS, KRS, AIMP1, and AIMP2) components of MSC were mixed in an equimolar ratio and were incubated in ice for 1 h before being injected into the column. Interactions between AIMP2 (residues 40–80), AIMP1 (residues 1–73), and His-RRS N-terminal helix (residues 1–74) were analyzed by a Superdex 75 10/300 column (GE Healthcare) at 4 °C.

GST Pull-Down Assay. Interactions between AIMP2 (residues 40–100) and the wild-type (or mutant) RQA1 complex were examined by GST-mediated pull-down assays. GST-AIMP2 (residues 40–100) was incubated with the ternary RQA1 complex containing wild-type or mutant AIMP1 in the presence of Glutathione Sepharose resin at 4 °C for 2 h. After extensive washing with PBS, the complex was eluted with 10 mM reduced glutathione.

SAXS. SAXS analyses of the human RQA1 complex (1, 2, 3, and 5 mg/mL) or the human RQA1–KA2 complex (1, 2, 3, and 5 mg/mL) were performed using the 4C SAXS II beamline of the Pohang Light Source II with 3 GeV power at the Pohang University of Science and Technology (Korea). All sample solutions were prepared in the buffer [25 mM Tris (pH 7.5), 150 mM NaCl, 5 mM DTT, 5% glycerol]. The light source from the in-vacuum undulator 20 (IVU 20: 1.4-m length, 20-mm period) of the Pohang Light Source II storage ring was focused using a vertical focusing toroidal mirror coated with rhodium and monochromatized with an Si (111) double crystal monochromator, yielding an X-ray beam wavelength of 0.675 Å (18.360 keV).

The X-ray beam size at the sample stage was 0.2 (V) × 0.6 (H) mm^2. A 2D charge-coupled detector (SX165, Mar USA, Inc.) was used with a sample-to-detector distance of 2.00 m. The magnitude of scattering vectors [$q = (4\pi/\lambda) \sin\theta$; where 2θ is the scattering angle and λ is the wavelength of the X-ray beam source] was $0.10\ nm^{-1} < q < 3.36\ nm^{-1}$. The scattering angle was calibrated with a polyethylene-*b*-polybutadiene-*b*-polystyrene block copolymer standard. Solution sample cells with 10-μm-thick mica windows, a volume of 50 μL, and an X-ray beam path length of 0.8 mm were used. To monitor radiation damage, the SAXS data were collected in five successive frames of 0.1 min each. All scattering measurements were carried out at 4 °C using an FP50-HL refrigerated circulator (JULABO).

Each 2D SAXS pattern was averaged circularly from the beam center and normalized to the transmitted X-ray beam intensity, which was monitored with a scintillation counter placed behind the sample. The scattering of the buffer solution was used as the experimental background. The theoretical SAXS curves were calculated from the crystal structures using the CRYSOL program (2).

Aminoacylation Assay. The arginylation or glutaminylation assay was carried out in a buffer containing 20 mM Hepes (pH 7.5), 20 mM KCl, 10 mM MgCl2, 4 mM DTT, 5 mM ATP, tRNA (yeast total tRNA, 4 mg/mL), and [^{3}H] arginine or glutamine (60 Ci/mmol). To obtain kinetic parameters (k_m, k_{cat}, and k_{cat}/k_m), human $tRNA^{Arg}$ (CCG), and human $tRNA^{Gln}$ (CUG) were synthesized by in vitro transcription and used with concentrations from 0.2–100 mM. Reactions were initiated by the addition of various RQA1 complexes or free RRS (or QRS) (40 nM) at 37 °C. Aliquots (15 uL) were taken at different time points and quenched on Whatman filter pads (catalog no. 1003323, grade 3, 2.3 cm) that were presoaked with 5% trichloroacetic acid (TCA). The pads were washed three times for 10 min each with 5% cold TCA and with 100% cold ethanol. The washed pads then were dried and placed into vials (Wheaton 986701) with 5 mL of the mixture solution. Radioactivity was quantified in a scintillation counter (Perkin-Elmer).

Western Blot. Purified GST (control), GST-RRS (Ha; residues 1–30), and GST-AIMP1 (N-140) were mixed with FLAG-RRS (Hb; residues 38–68) at a 1:1 molar ratio and were incubated at 4 °C for 3 h in the presence of glutathione resin. Beads bound to the samples were washed extensively with PBS and eluted with PBS containing 10 mM glutathione. Western blotting of GST, GST–RRS (Ha), GST–AIMP1 (N-140) and FLAG–RRS (Hb) were performed with α-GST and α-FLAG antibodies, respectively, following the transfer of electrophoretically separated proteins to PVDF membrane using standard immunoblotting techniques.

Circular Dichroism Analysis. The secondary structure of the N-terminal domain of RRS (N-74; Ha and Hb) was monitored by circular dichroism spectrophotometer (Jasco J-715) at wavelengths of 190–250 nm at 18 °C. RRS (N-74; 100 uM) was prepared in buffer containing 20 mM Tris-Cl (pH 7.5) and 100 mM NaCl.

Mutagenesis. All mutants used in this study were created by PCR-based methods. The mutant proteins were purified by affinity chromatography followed by anion exchange and gel-filtration chromatography, as described above. For gel-filtration analyses, four AIMP1 mutants (M1, M2, M3, and M4) were designed based on the interactions between AIMP1, RRS, and QRS. The second half (residues 44–72) of the N-terminal helix of AIMP1 were deleted in M1, and the first (residues 7–43) and second halves of the AIMP1 helix were exchanged in the M2 mutant. In M3, the first half (residues 1–38) of the N-terminal AIMP1 helix was deleted. In M4, the first half of the N-terminal AIMP1 helix (residues 1–30) was replaced by the leucine-zipper motif (residues 50–80) of AIMP2. The M1 and M2 mutants were inserted into the pET28a vector, and the M3 and M4 mutants were inserted into the pCDF vector. To generate the R1 mutant, five mutations (Lys50Asp, Tyr53Ala, Arg54Asp, Ile57Ala, and Glu65Arg) were made simultaneously in RRS. In the R2 mutant, the Ha helix of RRS (residues 1–35) was deleted. The R1 and R2 mutant were inserted into the pET-Duet vector. The AIMP2 leucine-zipper motif (residues 40–100) was inserted into the pGEX-4T3 vector, expressed in *E. coli* Rosetta (DE3), and then purified using GST-Sepharose resin with or without cleavage of the GST tag by thrombin. The Ha and Hb helices (residues 1–74) of RRS were inserted into the pET28a vector. The N-terminal helix of AIMP1 (residues 1–73) was inserted into the pCDF vector. RRS-Ha (residues 1–30) and AIMP1 (N-140; residues 1–140) were inserted into thepGEX-4T-3 vector, and RRS-Hb (residues 38–68) with a FLAG tag was insert into the pET28a vector.

1. Otwinowski Z, Minor W (1997) Processing of X-ray diffraction data collected in oscillation mode. *Methods Enzymol* 276(Pt A):307–326.

2. Svergun DI, Barberato C, Koch MHJ (1995) CRYSOL - a program to evaluate X-ray solution scattering of biological macromolecules from atomic coordinates. *J Appl Cryst* 28(Pt 6):768–773.

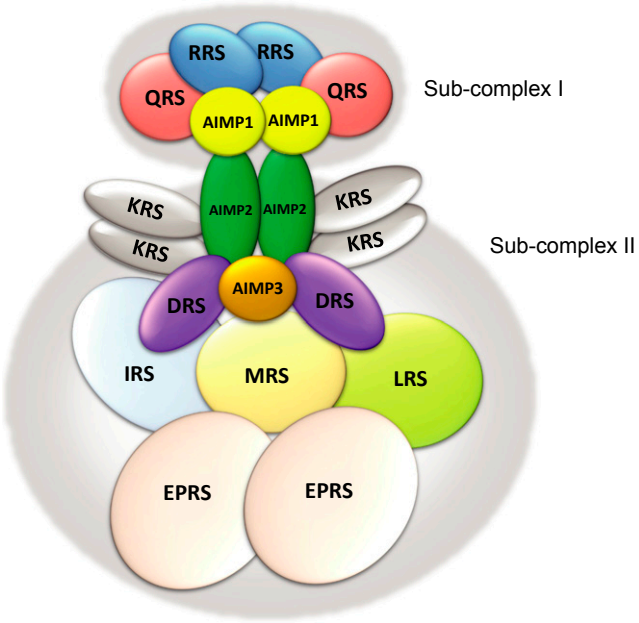

Fig. S1. A scheme for the architecture of the MSC complex. The overall architecture of the MSC is shown in a cartoon. In this model, the MSC is divided into the two subcomplexes. One subcomplex consists of RRS (2), QRS (2), and AIMP1 (2), and the other subcomplex consists of of KRS (4), AIMP2 (2), AIMP3 (1), MRS (1), EPRS (2), IRS (1), LRS (1), and DRS (2). [The numbers in parentheses indicate the number of components in the MSC from rabbit liver based on the reported biochemical analysis (1).] We note that the reported stoichiometry of QRS (one QRS) is different from our observations in the present study (two QRS); the model shown here contains two QRS molecules.

1. Kaminska M, et al. (2009) Dissection of the structural organization of the aminoacyl-tRNA synthetase complex. *J Biol Chem* 284(10):6053–6060.

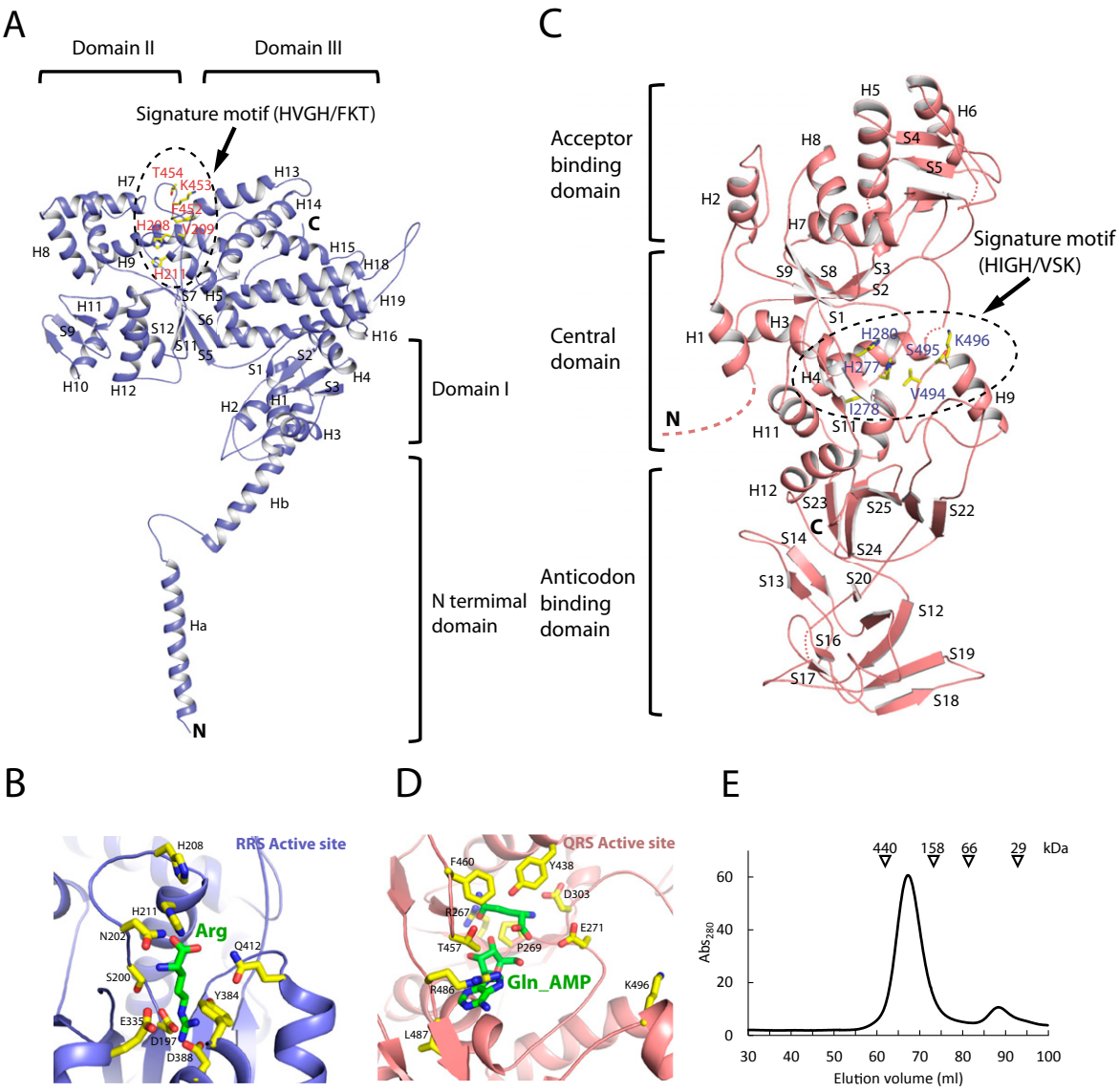

Fig. S2. Overall structures of human RRS and QRS core. (*A*) Overall structure of RRS in the human RQA1 complex. The N-terminal domain comprises helices Ha and Hb. Domain I folds into an α/β structure and binds to the D-loop of $tRNA^{Arg}$. Domain II is a catalytic domain that contains eight α-helices and eight β-strands; this domain binds to Arg, ATP, and the acceptor end of $tRNA^{Arg}$. Domain III comprises seven α-helices and recognizes the anticodon loop of $tRNA^{Arg}$. Residues in the signature motif of RRS are shown as yellow sticks. The N- and C-terminal ends of RRS are labeled. (*B*) Close-up view of the RRS active site. The figure is in same orientation as RRS in Fig. 1*B*, *Left*). (*C*) A ribbon diagram of the C-terminal core domain of QRS. The acceptor-binding domain forms an α/β fold and binds to the acceptor arm of $tRNA^{Gln}$. The central domain contains an active site that binds glutamine and ATP. The anticodon-binding domain binds to the anticodon loop of $tRNA^{Gln}$ and forms a β-barrel structure with 14 β-strands. The signature motif residues of QRS are shown as yellow sticks. The N- and C-terminal ends of QRS are labeled. (*D*) Close-up view of the QRS active site. The figure is in same orientation as RRS in Fig. 1*B*, *Left*. (*E*) Gel-filtration analysis of the RQA1 complex. The molecular weights of the standards are shown above the graph. The weight-average molecular mass of the peak was estimated to be 280 kDa.

Fig. S3. (Continued)

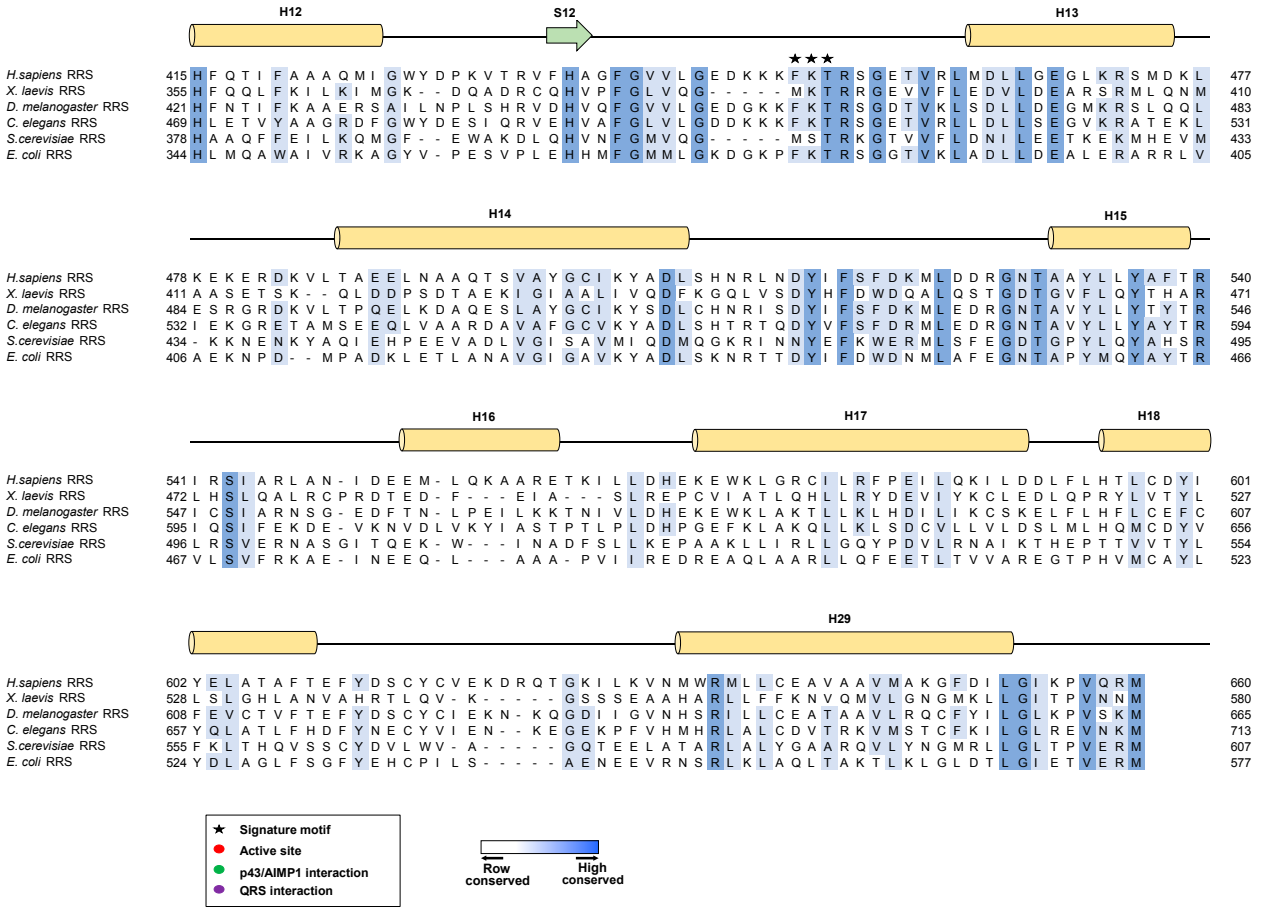

Fig. S3. (Continued)

B

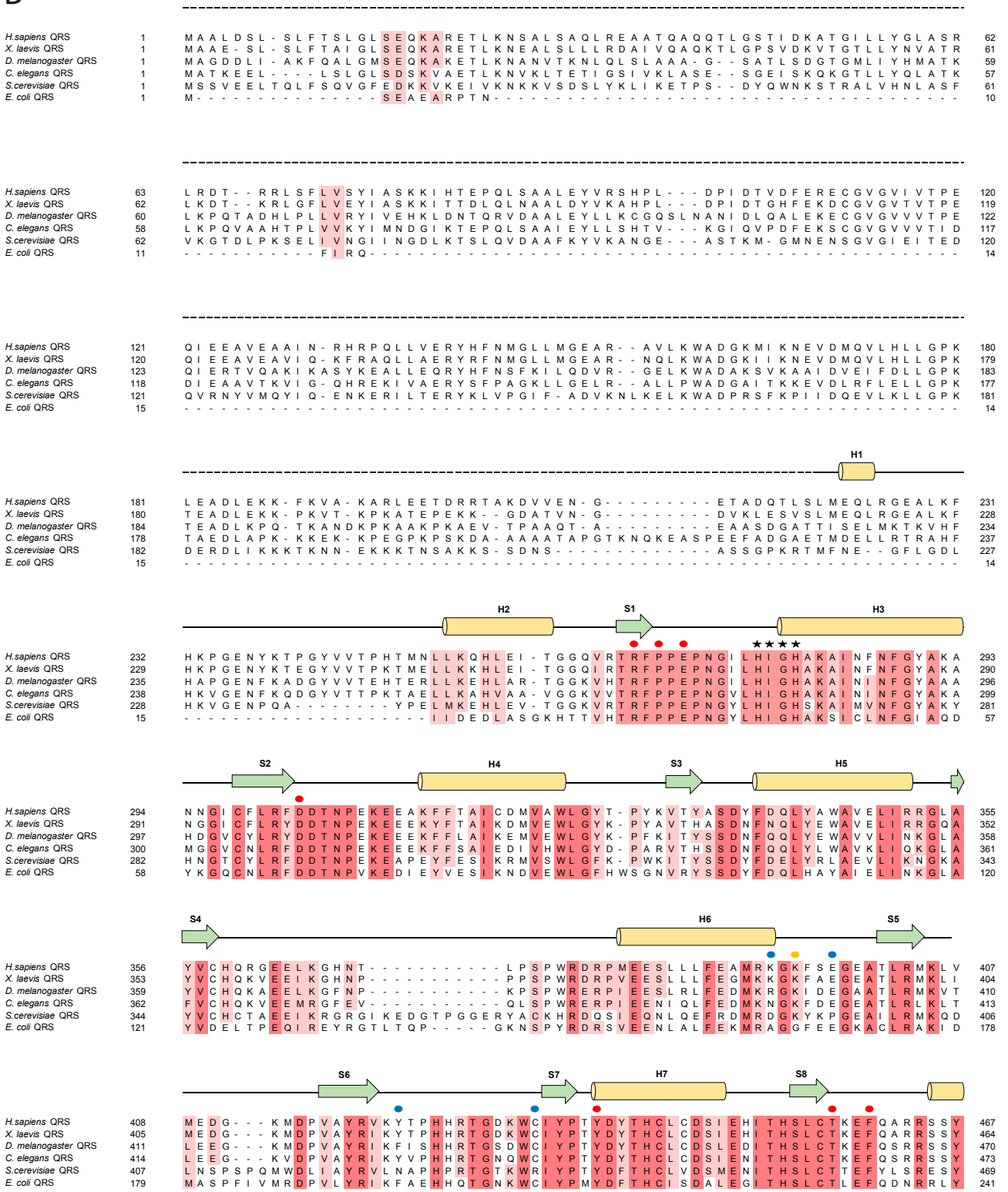

Fig. S3. (Continued)

Fig. S3. Structure-based sequence alignment of RRS and QRS homologs. (*A*) The secondary structure of human RRS is displayed above the sequences. The locations and functions of the key residues are highlighted and annotated. H, α-helix, S, β-sheet. (*B*) The secondary structure of human QRS is displayed above the sequences. The locations and functions of the key residues are highlighted and annotated.

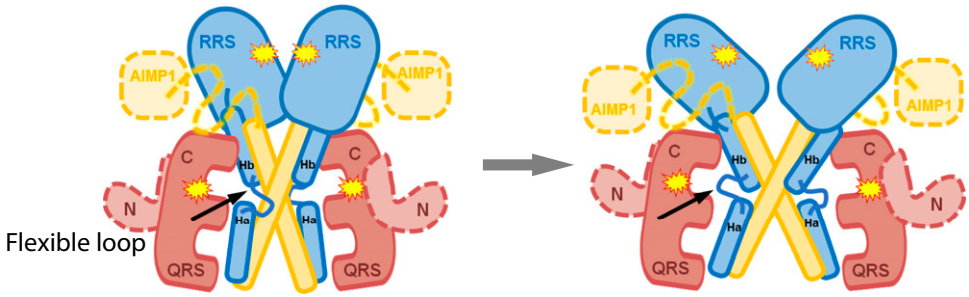

Fig. S4. Model of the conformational change in RRS in the hexameric subcomplex structure that allows $tRNA^{Arg}$ binding. The mobile loop (black arrow) between the Ha and Hb helices of RRS may allow rigid body movement of the RRS core and AIMP1 helix, which may result in the opening of the active site of RRS. The active sites are marked with stars.

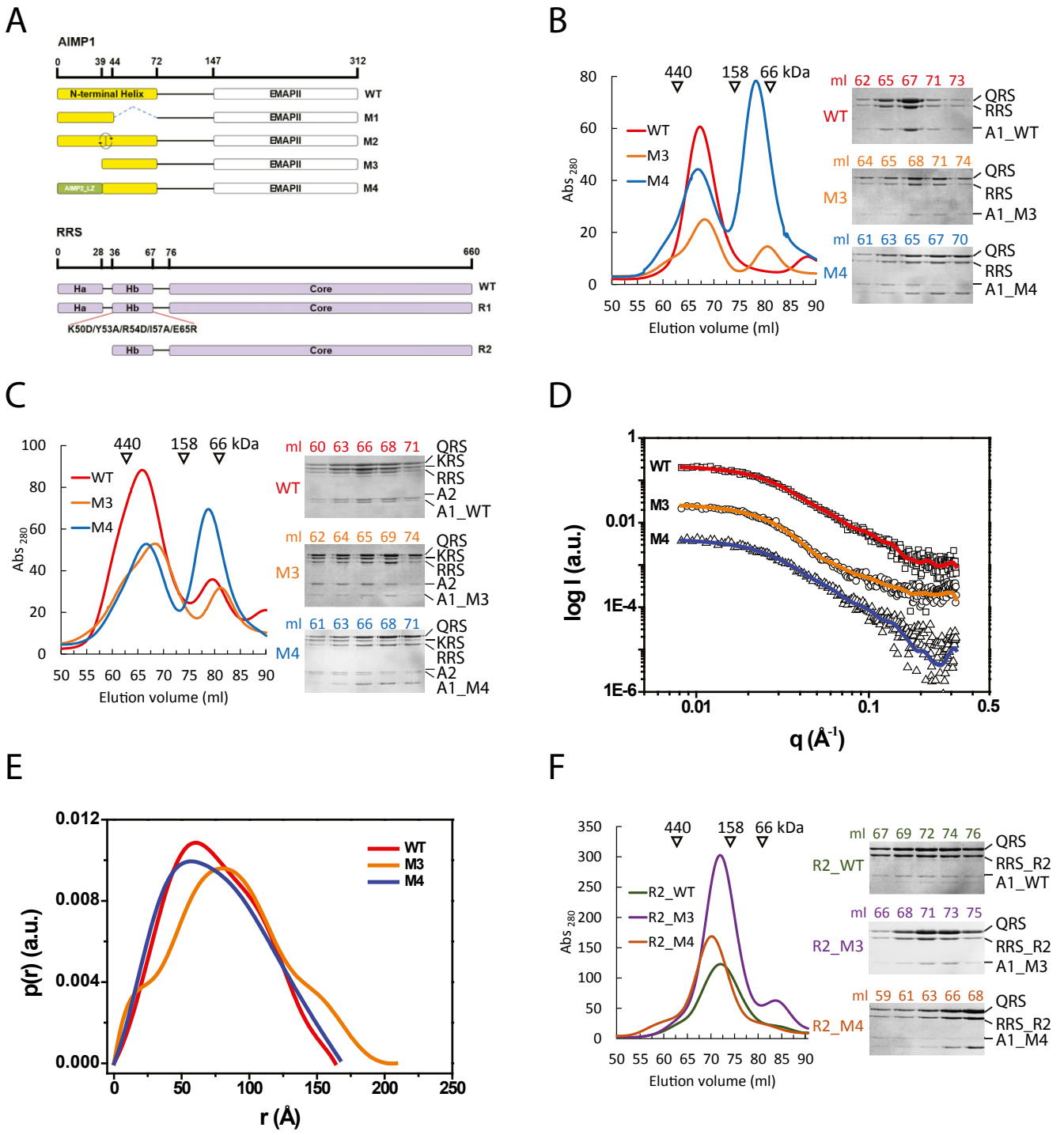

Fig. S5. Molecular assembly of the RQA1 or higher-order ARS subcomplex. (*A*) The schematic diagram of AIMP1 (M1, M2, M3, and M4) and RRS (R1 and R2) mutants used in this study. (*B*) Gel-filtration analyses of wild-type RQA1 (red), M3 mutant RQA1 (orange), and M4 mutant RQA1 (blue). The molecular weights of the standards are shown above the graphs. The elution volume of each lane is labeled on the top of gel in the color used in the graph. (*C*) Gel-filtration analyses of wild-type RQA1KA2 (red), M3 mutant RQA1KA2 (orange), and M4 mutant RQA1KA2 (blue). (*D*) The SAXS profile of the solution structure (1 mg/mL) of the RQA1 subcomplex containing wild-type AIMP1 (squares), the M3 (circles), or the M4 (triangles) mutant. The solid red (wild-type AIMP1), orange (M3 mutant), and blue (M4 mutant) lines are the theoretical SAXS curves obtained from the reconstructed structures of the hexameric forms of human ARS with lowest χ value using the ab initio shape-determination program DAMMIF (1). For clarity, each plot is shifted along the log I axis. (*E*) Pair distance distribution function $p(r)$ for the RQA1 complex containing wild-type AIMP1 (red) or the M3 (orange) or M4 (blue) mutant based on an analysis of the experimental SAXS data. (*F*) Gel-filtration analyses of the ternary complex containing the RRS R2 mutant, QRS, and wild-type AIMP1 (green) or the M3 (purple) or M4 (red) mutant.

1. Franke D, Svergun DI (2009) DAMMIF, a program for rapid ab-initio shape determination in small-angle scattering. *J Appl Cryst* 42(Pt 2):342–346.

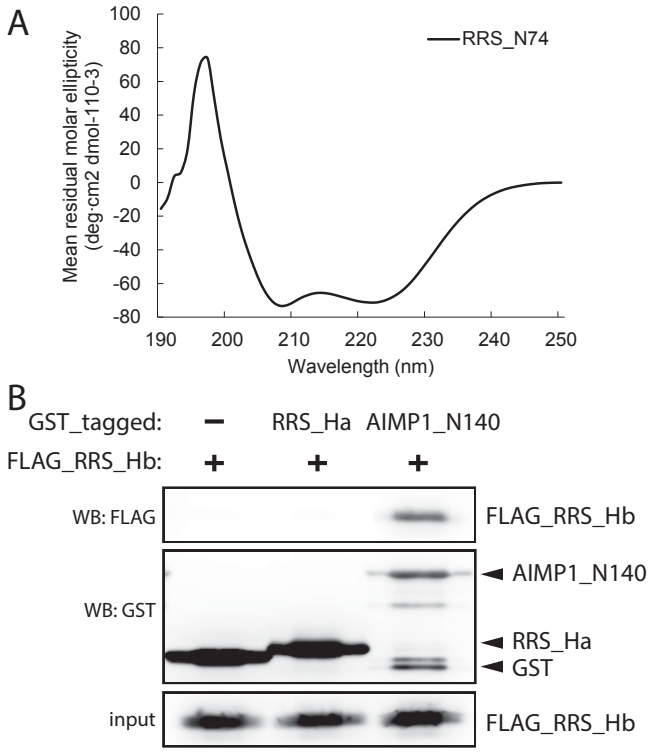

Fig. S6. The structural and biochemical features of the N-terminal helices of RRS. (*A*) Circular dichroism spectra of the N-terminal domain of RRS (N-74) showed that the region forms the α-helix structure. Structure of the RRS (N-74) fragment was monitored by CD spectrophotometer (Jasco J-715) at wavelengths of 190–250 nm at 18 °C. (*B*) Western blot of the GST-RRS (Ha) and FLAG-RRS (Hb). Purified GST-tagged protein was mixed with FLAG-RRS (Hb) at a 1:1 molar ratio and was incubated at 4 °C for 3 h in the presence of glutathione resin. Blots were probed with antibody (α-GST or α-FLAG) directed against GST (control), GST-RRS (Ha), GST-AIMP1 (N-140), and FLAG-RRS (Hb).

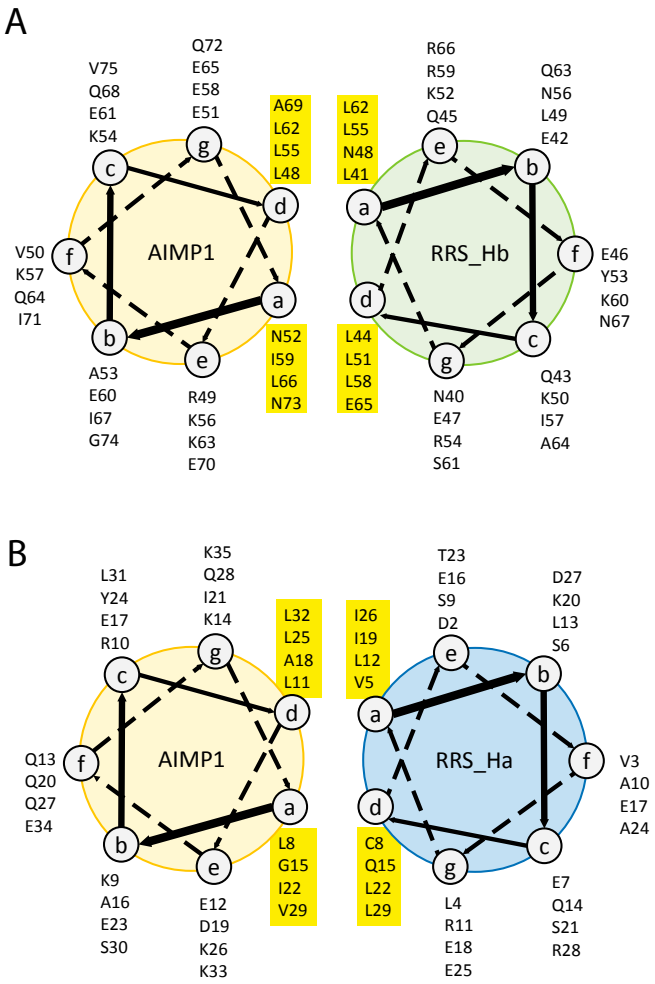

Fig. S7. Helical wheel diagram of the coiled-coil interactions between the N-terminal helices of AIMP1 and RRS. (*A*) The parallel coiled-coil interactions between the Hb helix of RRS and the second half of the AIMP1 helix. (*B*) The coiled-coil interface between the Ha helix of the symmetry-related RRS protein and the first half of the AIMP1 helix. The two helices are directed in a parallel manner. The leucine-zipper interactions are highlighted in yellow.

Table S1. Data collection and refinement statistics for RRS-QRS-AIMP1

Data collection	
Space group	$C222_1$
Cell dimensions	
a, *b*, *c*, Å	102.7, 313.3, 161.8
α, β, γ, °	90, 90, 90
Resolution, Å*	50–3.85(3.92–3.85)
R_{sym}	11.5(79.9)
$I/\sigma I$	22.3(2.9)
Completeness (%)	99.5(99.8)
Redundancy	5.1(5.0)
Refinement	
Resolution, Å	37.9–4.0
No. reflections	15,364
$R_{work}/R_{free,}$ %	23.7/28.7
No. atoms†	
Protein	10,246
B-factors, Å^2	
RQA1	155.1
RRS	166.9
QRS	140.1
AIMP1	159.1
Rmsd	
Bond lengths, Å	0.004
Bond angles, °	0.874

*Values in parentheses are for highest-resolution shell.
†The final model consists of residues 2–660 of RRS, residues 220–771 of QRS, and residues 5–80 of AIMP1 with 95.1% favored and 4.9% outliers in Ramachandran plot. The N terminus of QRS and C terminus of AIMP1 were not visible.

Table S2. Structural parameters obtained from the SAXS data of the MSC subcomplex in solution

Sample	$R_{g,G}$, Å*	$R_{g,p(r)}$, Å†	D_{max}, Å†
RQA1 subcomplex			
RQA1 trimeric crystal	49.00 ± 0.05	49.06 ± 0.04	167.8
RQA1 hexameric crystal	56.20 ± 0.01	56.26 ± 0.04	187.6
RQA1_WT	56.40 ± 0.49	57.91 ± 0.59	163.5
RQA1_M3	67.09 ± 0.96	67.14 ± 1.38	208.5
RQA1_M4	58.52 ± 0.54	58.60 ± 0.26	168.9
RQA1-KA2 subcomplex			
RQA1-KA2	77.10 ± 1.48	80.48 ± 0.22	258.4

*Radius of gyration obtained from the scattering data by the Guinier analysis.
†$R_{g,p(r)}$ (radius of gyration) and D_{max} (maximum dimension) were calculated from the *p*(r) function by the program GNOM (1).

1. Svergun DI (1992) Determination of the regularization parameter in indirect-transform methods using perceptual criteria. *J Appl Cryst* 25(Pt 4):495–503.

Table S3. Kinetic parameters for tRNA of RRS and QRS in the MSC subcomplex

Enzyme	Human $tRNA^{Arg}$ or $tRNA^{Gln}$	K_m, mM	k_{cat}/s	k_{cat}/K_M·s^{-1}·mM^{-1}
RRS/QRS				
Full length	RRS	4.529 ± 0.187	1.115 ± 0.059	0.246
Full length	QRS	4.021 ± 0.112	1.27 ± 0.087	0.316
RQA1 subcomplex				
R-Q-A1(WT)	RRS	4.826 ± 0.155	1.121 ± 0.078	0.232
	QRS	3.320 ± 0.091	1.15 ± 0.021	0.346
R-Q-A1(M3)	RRS	N.D.	N.D.	N.D.
	QRS	3.126 ± 0.035	1.031 ± 0.008	0.330
R-Q-A1(M4)	RRS	N.D.	N.D.	N.D.
	QRS	3.408 ± 0.038	1.09 ± 0.011	0.320
R(R2)-Q-A1(WT)	RRS	4.206 ± 0.053	1.125 ± 0.017	0.267
	QRS	3.156 ± 0.037	0.958 ± 0.016	0.304
R(R2)-Q-A1(M3)	RRS	4.044 ± 0.073	1.068 ± 0.058	0.264
	QRS	3.956 ± 0.041	1.163 ± 0.007	0.294
R(R2)-Q-A1(M4)	RRS	4.018 ± 0.097	1.077 ± 0.098	0.268
	QRS	3.325 ± 0.032	0.923 ± 0.018	0.278
RQA1–KA2 subcomplex				
R-Q-A1-K-A2(WT)	RRS	5.370 ± 0.057	1.201 ± 0.021	0.224
	QRS	7.674 ± 0.070	2.23 ± 0.013	0.291
R-Q-A1(M3)-K-A2	RRS	N.D.	N.D.	N.D.
	QRS	7.938 ± 0.159	1.807 ± 0.026	0.228
R-Q-A1(M4)-K-A2	RRS	N.D.	N.D.	N.D.
	QRS	6.912 ± 0.132	1.512 ± 0.063	0.219

N.D., not detected.